RSC Advances

PAPER

View Article Online
View Journal | View Issue

Cite this: *RSC Adv.*, 2018, **8**, 34650

Water adsorbancy of high surface area layered double hydroxides (AMO-LDHs)†

Chunping Chen, Kanittika Ruengkajorn, Jean-Charles Buffet and Dermot O'Hare *

Received 14th August 2018
Accepted 25th September 2018

DOI: 10.1039/c8ra06822d

rsc.li/rsc-advances

Understanding the water adsorbancy of highly dispersed, high surface area layered double hydroxide (LDH) is of great importance as it directly relates to their hydrophobicity and subsequent use as additives in LDH-polymer nanocomposites. In this study, we have investigated the water vapour uptake response of highly dispersed, high surface area aqueous miscible organic-LDHs (AMO-LDHs) in two relative humidity atmospheres (RH99 and RH60) at 20 °C. We observed that AMO-$Mg_3Al–CO_3$ and AMO-$Zn_2MgAl–CO_3$ exhibited very high water vapour uptake in an RH99 atmosphere at 20 °C (56 wt% and 20 wt% for $Mg_3Al–CO_3$ and $Zn_2MgAl–CO_3$ LDH respectively after 120 h). The crystallinity in both *ab*-plane and *c*-axis of the LDHs increased with increasing exposure uptake. The water vapour adsorption capacity of the AMO-LDHs can be dramatically reduced by treatment with stearic acid.

Introduction

Layered double hydroxide (LDH) is an important class of anionic clay consisting of positively charged brucite-like layer with negatively charged interlayer of anions and water molecules. The general formula of LDH can be expressed as $[M^{z+}_{1-x}M'^{y+}_{x}(OH)_2](X^{n-})_{a/n}\cdot bH_2O$, wherein most commonly the M and M′ are metal cations, typically $z = 2$, $y = 3$, $0 < x < 1$, $b = 0$–1, giving $a = z(1 - x) + xy - 2$; X^{n-} is an organic or inorganic anion.[1–3] Their flexible composition, uniform metal dispersion and tuneability of acidity and basicity sites enable LDH to be used in catalysis.[4–7] Strong positively charged surface and high surface area lead LDH to have excellent performance in adsorption.[8,9] Furthermore, the 2D layer structure and controllable layer thickness give LDH promising gas barrier applications.[10–12] However, due to the potential for strong hydrogen bonding interactions, LDHs present a very hydrophilic surface, leading to serious aggregation of the primary particles and significant water vapour adsorption. O'Hare and co-workers have developed a general and simple method, so called Aqueous Miscible Organic Solvent Treatment method (AMOST), to address the aggregation issue and achieve a new class of LDH (AMO-LDH) that exhibit high specific surface area, pore volume and good dispersibility in non-polar solvents and polymers.[13–17] However, these materials can incorporate high water content through rapid water vapour adsorption which needs to be addressed to meet applications such as pharmaceutical delivery or as additives in polymers.

Water vapour ab/adsorption during synthesis, storage and transport can greatly affect the properties of a material such as poor phase purity and crystallinity and/or physical/chemical instability. There are an increasing number of studies on water stability of inorganic materials, particularly perovskites, metal–organic frameworks (MOF), food, and pharmaceutical solids.[18–23] However, there is a dearth of reports on the water vapour uptake responses of LDH materials.[24–26] Yun *et al.* demonstrated that increasing the layer charge by increasing aluminium content can lead to larger amounts of surface water.[25] Iyi *et al.* investigated the hydration of LDHs with different Mg/Al ratios and anions in various relative humidities.[24] They found that LDHs containing I^-, SO_4^{2-} and ClO_4^- showed an hydrate phase with discrete basal-spacing expansion in high RH due to the intercalation of one water layer. For CO_3^{2-} LDH, no apparent changes in basal spacing can be observed.

In this study, AMO-$Zn_2MgAl–CO_3$ and AMO-$Mg_3Al–CO_3$ were synthesised and the time-dependence of their water vapour uptake investigated in two relative humidity atmospheres (RH99 and RH60). The structure, lattice dimensions, crystallinity, thermal decomposition and specific surface area were studied using XRD, FTIR, TGA and N_2 BET. Furthermore, we developed a surface modification of AMO-LDHs with stearic acid to control the hydrophilicity.

Experimental

Materials

Magnesium nitrate hydrate ($Mg(NO_3)_2\cdot 6H_2O$, >99.0%), Aluminium nitrate nonahydrate ($Al(NO_3)_3\cdot 9H_2O$, >98%), stearic acid and zinc nitrate hexahydrate ($Zn(NO_3)_2\cdot 6H_2O$, 99%) were purchased from Sigma-Aldrich. Sodium carbonate (Na_2CO_3,

Chemistry Research Laboratory, Department of Chemistry, University of Oxford, 12 Mansfield Road, Oxford, OX1 3TA, UK. E-mail: dermot.ohare@chem.ox.ac.uk

† Electronic supplementary information (ESI) available: TGA, FTIR, PXRD, N_2 adsorption and desorption isotherm, specific BET surface area and pore volume, ^{27}Al SSNMR spectroscopy. See DOI: 10.1039/c8ra06822d

99.6%) was purchased from Acros Organics. Nitric acid (HNO_3, 70%) and Sodium hydroxide (NaOH) was purchased from Fisher Chemicals.

Synthesis of AMO-Mg_3Al–CO_3-LDH

The metal precursor solution containing 19.2 g $Mg(NO_3)_2 \cdot 6H_2O$, 9.38 g $Al(NO_3)_3 \cdot 9H_2O$ and 100 mL water was added drop-wise into Na_2CO_3 base solution (100 mL water with 5.3 g Na_2CO_3, pH is adjusted to be 10 by 10% HNO_3 solution) within 1 h. The pH was kept constant around 10.0 by drop wise addition of a 4.0 M NaOH solution. After stirring for 16 h at room temperature, the mixture was filtered and washed with deionised (DI) water until pH 7. The wet LDH solid was dispersed in ethanol (1000 mL) followed by re-dispersion in fresh ethanol (600 mL) and stirred at room temperature for 4 h. The AMO-LDH was then isolated by filtration, washed with 400 mL of ethanol and dried under vacuum overnight. AMO-Mg_3Al–CO_3-LDH has the composition $[Mg_{0.75}Al_{0.25}(OH)_2](CO_3)_{0.125} \cdot 0.5(H_2O) \cdot 0.04$(ethanol).

Synthesis of AMO-Zn_2MgAl–CO_3-LDH

The general procedure is shown as following: the metal precursor solution containing 6.4 g $Mg(NO_3)_2 \cdot 6H_2O$, 14.68 g $Zn(NO_3)_2 \cdot 6H_2O$, 9.38 g $Al(NO_3)_3 \cdot 9H_2O$ and 100 mL water was added drop-wise into Na_2CO_3 base solution (100 mL water with 5.3 g Na_2CO_3) within 1 h. The pH was kept constant around 10.0 by drop wise addition of a 4.0 M NaOH solution. After stirring for 16 h at room temperature, the mixture was filtered and washed with deionised (DI) water until pH 7. The wet solid LDH was treated with ethanol by using AMO method. The AMO-LDH was isolated by filtration and dried under vacuum overnight. AMO-Zn_2MgAl–CO_3 has the composition $[Zn_{0.5}Mg_{0.25}Al_{0.25}(OH)_2](CO_3)_{0.125} \cdot 0.06(H_2O) \cdot 0.031$(ethanol).

Water vapour uptake measurements

The water vapour uptake measurements were carried out according to a modified Callahan's method.[27] The water vapour uptake was measured in a sealed box at room temperature (20 °C). The relative humidity RH99 and RH60 were generated by saturated solution of KNO_3 and $Mg(NO_3)_2$ respectively. The detailed measurement procedures are shown in the ESI.†

Synthesis of stearic acid modified Zn_2MgAl–CO_3 AMO-LDH

Various amounts of stearic acid (0.25, 0.5, 1 and 2 mmol g^{-1} LDH) were dissolved in 300 mL of ethanol. 3 g of AMO-Zn_2MgAl–CO_3 was introduced into a stearic acid solution and mixed using a homogeniser for 30 minutes. The obtained suspension was then refluxed at 80 °C for 16 h. The solid was collected by filtration and washed with 600 mL of ethanol followed by drying in an oven at 150 °C for further characterisations and testing. The obtained samples are named as ZMA-SA*x* where ZMA is AMO-Zn_2MgAl–CO_3 and *x* the amount of stearic acid (SA).

Results and discussion

AMO treatment

AMOST treatment of Mg_3Al–CO_3 and Zn_2MgAl–CO_3 produces high surface area and highly dispersed AMO-LDHs with the chemical composition $[Mg_{0.75}Al_{0.25}(OH)_2](CO_3)_{0.125} \cdot 0.5(H_2O) \cdot 0.04$(ethanol) and $[Zn_{0.5}Mg_{0.25}Al_{0.25}(OH)_2](CO_3)_{0.125} \cdot 0.06(H_2O) \cdot 0.031$(ethanol) for AMO-$Mg_3Al$–$CO_3$ and AMO-Zn_2MgAl–CO_3, respectively (Table S1†). N_2 BET studies show that the specific surface areas for AMO-Mg_3Al–CO_3 and AMO-Zn_2MgAl–CO_3 are 376 and 115 $m^2\ g^{-1}$, respectively. These values are 5–10 times the values that would be measured for a conventionally prepared LDHs using co-precipitation from water.

Time-dependent water vapour uptake response

The water content of AMO-Mg_3Al–CO_3 and AMO-Zn_2MgAl–CO_3 after drying in vacuum overnight was determined using TGA (Fig. S1†). Both AMO-Mg_3Al–CO_3 and AMO-Zn_2MgAl–CO_3 release high water/AMO solvent corresponding to 21.6 and 11.7 wt% based on a dry weight, respectively. The time-dependence of water vapour uptake was measured in different relative humidity atmospheres. As shown in Fig. 1(a), AMO-Zn_2MgAl–CO_3 adsorbed less than 5 wt% water upon exposition to a low relative humidity, RH60. However, when exposed at high humidity RH99 (Fig. 1(b)), the water vapour uptake dramatically increased up to 20 wt%. AMO-Mg_3Al–CO_3 (Fig. 1(c)) can adsorb water vapour continuously up to 56 wt% based on a dry weight in RH99 humidity over 96 h. This is corresponding to 36 wt% of EMC (equilibrium water content) which belongs to the Class IV (very hygroscopic) according to Callahan's hygroscopicity classification.[27] We attribute the higher water vapour uptake to the higher surface area for AMO-Mg_3Al–CO_3 (376 $m^2\ g^{-1}$) compared to AMO-Zn_2MgAl–CO_3 (115 $m^2\ g^{-1}$). Particle size was also shown to affect water vapour uptake response. As shown in Fig. S2,† both platelet samples have similar surface areas, but the sample with the smaller size

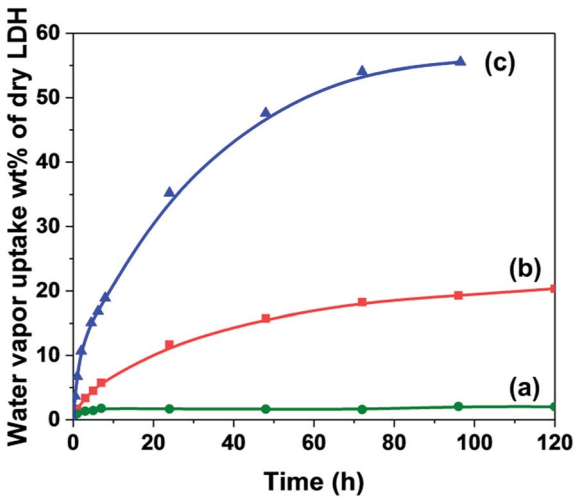

Fig. 1 Time dependence of water vapour uptake for: (a) AMO-Zn_2MgAl–CO_3 in RH60 (b) AMO-Zn_2MgAl–CO_3 in RH99 and (c) AMO-Mg_3Al–CO_3 in RH99.

platelets exhibits to higher water vapour uptake owing to their higher surface energy which favours forming hydrogen bonding with water molecules.

Weight losses of AMO-Zn_2MgAl–CO_3 before and after water vapour adsorption were also measured using TGA as shown in Fig. S3† and collated in Table S2.† Weight loss below 70 °C is mainly attributed to the release of the interparticle water[25] and AMO-solvent.[15] The weight loss between 70–180 °C is due to the loss of surface bound water and/or AMO solvent and possibly partially de-hydroxylation.[25,28] We found that AMO-Zn_2MgAl–CO_3 contained very low quantities of interparticle pore water and AMO-solvent (1.2 wt% of dry LDH). However, after exposure to at RH99 atmosphere at 20 °C the interparticle pore water dramatically increases to 9.5 and 14.6 wt% after 24 and 72 h, respectively. The water molecules might not only condense in the interparticle space but also diffuse into the surface and the interlayer as observed with amount of surface water increasing from 10.5 to 13.1 wt% after 72 h in RH99.[24]

These results are consistent with those found using XRD. Fig. S4 and Table S3† show no apparent changes in lattice parameters (*a* and *c*) for AMO-Zn_2MgAl–CO_3 and AMO-Mg_3Al–CO_3 after water vapour adsorption. However, the broadness of both (003) and (110) Bragg reflections decrease after water vapour adsorption. The mean crystalline domain length (CDL) (Table 1) calculated using the Scherer equation reveals that the crystallinity along *c*-axis and in the *ab*-plane gradually increases with exposure time. Along the *c*-axis, the crystalline domain length increases after water vapour adsorption for 120 h from 7.9 to 8.4 nm and 2.9 to 4.6 nm for AMO-Zn_2MgAl–CO_3 and AMO-Mg_3Al–CO_3, respectively.

We also observed that the crystalline domain length (CDL) of AMO-LDH samples in the *ab*-plane dramatically increases with increased water vapour exposure as shown in Table 1 and Fig. 2. The CDL is calculated to be more than 3 and 2 nm larger than that of anhydrous AMO-Zn_2MgAl–CO_3 and AMO-Mg_3Al–CO_3 respectively. These findings may be the contributing factor to the observed decrease of the surface area as shown in Fig. S5,† suggesting the possibility for rearrangement of the LDH structure *via* dissolution–recrystallization of metal hydroxide layers during the water vapour adsorption.

Table 1 Crystalline domain length of AMO-LDHs before and after exposure to atmosphere with RH99 at 20 °C

		Mean crystalline domain length[a] (nm)	
	Exposing time (h)	*c*-axis	*ab*-plane
Zn_2MgAl–CO_3AMO-LDH	0	7.9	59.5
	5	8.0	60.2
	24	8.2	61.6
	72	8.2	62.5
	120	8.4	62.9
Mg_3Al–CO_3AMO-LDH	0	2.9	20.5
	120	4.6	22.6

[a] Crystalline domain length (CDL) along *c*-axis is calculated from Scherer equation using full width at half-maximum (FWHM) of the (003) Bragg reflection; the CDL in *ab*-plane is calculated from Scherer equation using full width at half-maximum (FWHM) of the (110) Bragg reflection.

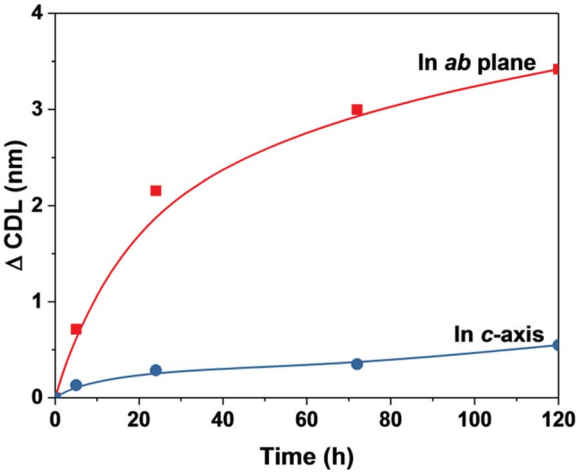

Fig. 2 Change in crystalline domain length (ΔCDL) in *ab*-plane and *c*-axis for AMO-Zn_2MgAl–CO_3 as a function of exposure time in an RH99 atmosphere.

FTIR is of great interest to study the adsorbed water molecules in the AMO-LDH and their interaction with AMO-LDH structure. Fig. S6† shows a broad absorption between 400–1100 cm^{-1} which is assigned to the O–M–O bending, M–O stretching and deformation, M–OH deformation and ν_4 and ν_2 vibrations of CO_3^{2-}.[1,29] The band at 1367 cm^{-1} is ascribed to the ν_3 of the CO_3^{2-} in a symmetric environment. The band at 1639 cm^{-1} can be assigned to an interlayer water bending mode.[1] This band becomes more prominent after exposure in an RH99 atmosphere. The broad absorbance in the range of 2800–3800 cm^{-1} is due to stretching of H-bonded OH groups. The band becomes broader with increasing exposing time. By Gaussian peak shape deconvolution on the absorbance mode, more detailed information can be revealed as shown in Fig. 3. There are three main absorption bands (B1: 3052–3270 cm^{-1}, B2: 3279–3410 cm^{-1}, B3: 3470–3530 cm^{-1}), which are assigned to the carbonate, H_2O/H_2O–H_2O bridging mode, the hydrogen bonding of water in highly structured environment in the interlayer galleries and the M–OH stretching with water molecules, respectively.[1,29,30] All the –OH stretching bands are shifted to higher wavenumber, which might be due to the stronger hydrogen bonding with a larger concentration of water molecules.

Inhibition of water vapour adsorbance

As discussed above, LDHs, especially those with high surface areas and small particle sizes, exhibit very high water saturation content and a rapid water vapour adsorption rate. We have investigated simple methods to alleviate this issue. Stearic acid is commonly used as a surface modifier for fillers such as calcium oxide, alumina, and magnesium hydroxide to reduce the water vapour adsorption and increase their compatibility with non-polar materials.[31–34] Traditionally, LDHs are modified with fatty acids (in their salt form), requiring deprotonation

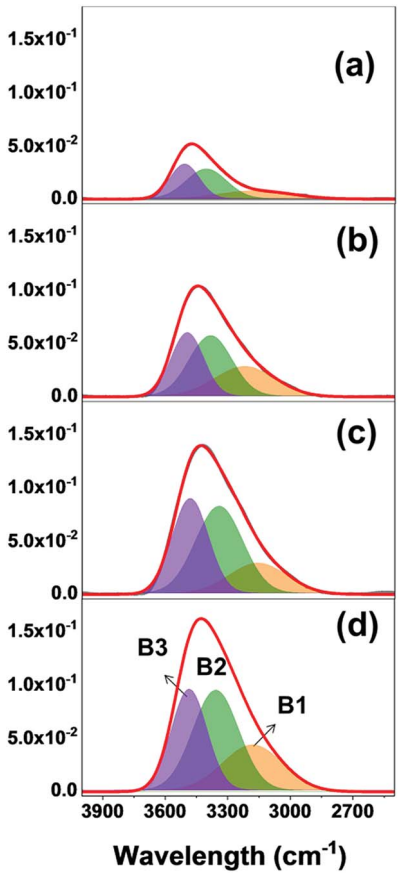

Fig. 3 FTIR spectra (absorbance mode) of AMO-Zn_2MgAl–CO_3 after exposure to an RH99 atmosphere; (a) 0 h, (b) 24 h, (c) 72 h and (d) 120 h.

before use. In this study, the stearic acid was introduced to the AMO-LDHs by post treating in ethanol slurry at 80 °C.

The XRD data for AMO-Zn_2MgAl–CO_3 before and after treatment with different loadings of stearic acid are shown in Fig. 4. The XRD of samples with low stearic acid loadings are consistent with single phase pure LDH exhibiting a series of (00l) Bragg reflections and two well-separated (110) and (113) Bragg reflections at $2\theta = 60°$ and 62°, that data indicates there is no free crystalline stearic acid present in these samples. The interlayer spacing (d(003)) remained the same as the pristine LDH, confirming that the stearic acid is grafted on the surface of LDH instead of intercalating into the interlayer galleries. When the stearic acid loading is higher than 2 mmol g^{-1}-LDH, additional reflections at lower 2θ values can be observed. These features could be assigned to crystalline stearic acid. The amount of stearic acid grafted onto the LDH can be is estimated from the TGA data (Table S4†). At low stearic acid treatment ratios most of it is grafted onto the LDH. Dosing the LDHs with 1.0 mmol stearic acid per gram LDH (28 wt%) only resulted in 11 wt% stearic incorporation (by TGA). Dosing the LDHs with 2.0 mmol stearic acid per gram LDH (56 wt%) resulted in 27% incorporation but with substantial crystallisation of stearate acid.

Fig. 5 shows the FTIR spectra of AMO-Zn_2MgAl–CO_3 modified with different loadings of stearic acid. The characteristic bands assignable to stearic acid can be found in all modified

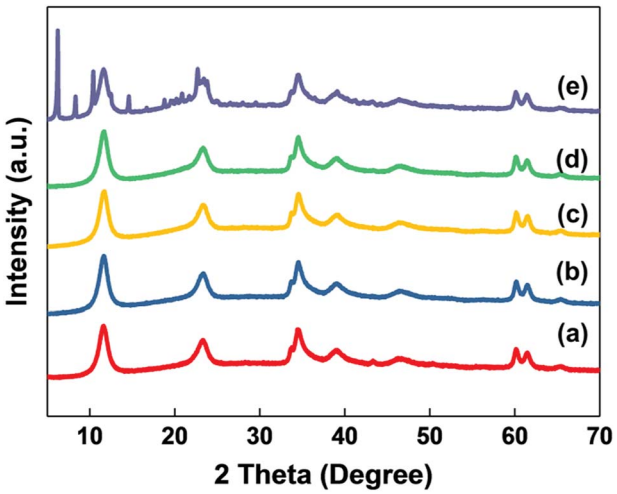

Fig. 4 XRD patterns of (a) AMO-Zn_2MgAl–CO_3, (b) ZMA-SA0.25, (c) ZMA-SA0.5, (d) ZMA-SA1.0 and (e) ZMA-SA2.0.

samples at 2920, 2852, 1545 and 1472 cm^{-1}, these features correspond to CH_2 antisymmetric and symmetric stretching, COO^- antisymmetric stretching and a CH_2 scissor mode, respectively.[35] These absorbances grow in intensity with increasing stearic acid loading.

Furthermore, the H_2O bending mode at 1639 cm^{-1} disappears and the –OH stretching band in the region of 2800–3800 cm^{-1} becomes much lower in intensity than a pristine LDH. The data indicates that the stearic acid treatment imparts hydrophobicity and so can effectively prevent water molecules penetrating the LDH layers. Stearic acid commonly displays a carbonyl stretching band due to dimerisation at 1698 cm^{-1} instead of a carboxylate band at 1575 cm^{-1}.

In this study, a carbonyl band is not observed in all stearic acid modified samples. We believe that the stearic acid is deprotonated by the basic LDH surface and so dimerisation is inhibited. Similar behaviour has been observed for other inorganic basic materials such as $Mg(OH)_2$ and $CaCO_3$.[31,32,35]

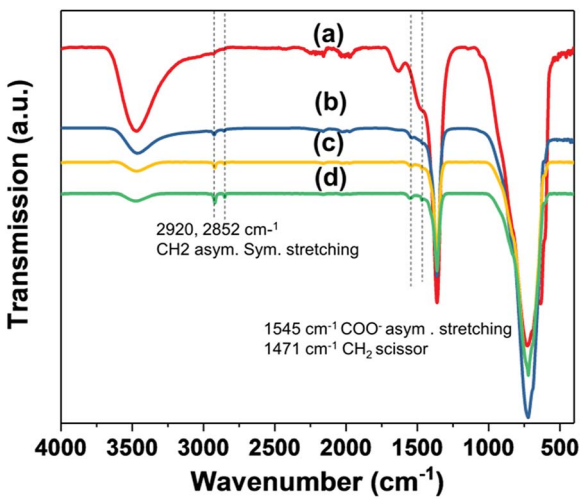

Fig. 5 FTIR spectra of (a) AMO-Zn_2MgAl–CO_3, (b) ZMA-SA0.25, (c) ZMA-SA0.5, (d) ZMA-SA1.0.

The solid state ^{27}Al NMR spectroscopic data are shown in Fig. S7.† AMO-Zn_2MgAl–CO_3 exhibit a resonance at *ca.* −15 ppm typical of octahedral Al sites (O_h) within the LDH. After surface modification with stearic acid, an extra low intensity resonance at *ca.* 50 ppm (tetrahedral Al sites (T_d)) can be observed, indicating that some Al^{3+} ions migrate from octahedral sites to complex with stearate anions. The ratio of octahedral to tetrahedral Al^{3+} sites was calculated by integrating the NMR resonances and are collated in Table S5.† The Al^{3+} T_d;O_h site ratio increases from 100 : 0.5 to 100 : 15 after stearic acid treatment with a loading of 0.25 mmol g^{-1}-LDH. This data confirms that stearate has successfully been grafted onto the LDH surface. This conclusion is also consistent with the N_2 BET surface area (Fig. S8†) and pore volume (Fig. S9†) results. Both the N_2 specific BET surface area and pore volume slightly decrease with increasing loading with stearic acid up to 1 mmol g^{-1}-LDH (attributed to surface coverage of the modifier). We observe that the particles become significantly aggregated if the loading reaches 2 mmol g^{-1}-LDH; resulting in a dramatic drop in surface area and pore volume.

The water contents of all samples were measured using TGA at 180 °C. The water content of AMO-Zn_2MgAl–CO_3 is *ca.* 11.7 wt% of dry basis and after thermal treatment at 150 °C is still 2.4 wt%. For stearic acid treated samples, the water content dramatically reduces from 2.4 to 0.9 wt% as a function of stearic acid loading from 0 to 2 mmol g^{-1}-LDH. The water vapour uptake response of AMO-Zn_2MgAl–CO_3 after surface treatment with stearic acid was investigated by exposing the modified samples to a RH99 atmosphere at 20 °C.

As shown in Fig. 6, the stearic acid modified AMO-Zn_2MgAl–CO_3 has a much reduce hydrophilicity with dramatically reduced water vapour affinity. With a stearic acid loading of only 0.25 mmol g^{-1}-LDH, the water vapour uptake after 96 h can be reduced from 34 to 18 wt% of dry LDH. Further increasing the stearic acid loading up to 2 mmol g^{-1}-LDH can effectively reduce the saturation water capacity below 8 wt% of dry LDH after 150 h. These results suggest that the use of stearic acid for surface modification on LDH can provide a viable strategy to obtain LDH with less water content and low water vapour uptake, which is promising in the water sensitive applications.

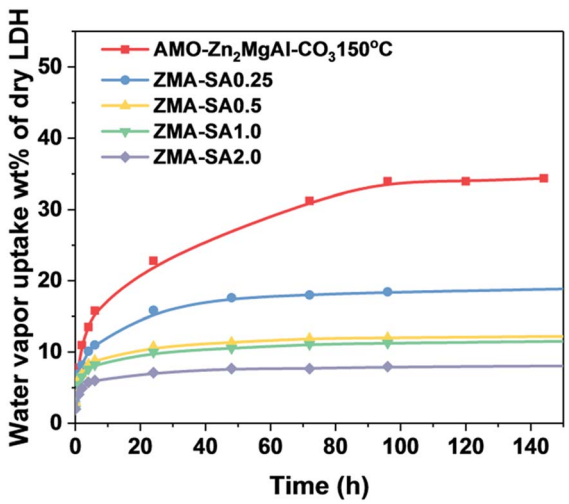

Fig. 6 Time dependence of water vapour uptake for AMO-Zn_2MgAl–CO_3 with and without stearic acid modification after drying at 150 °C.

Conclusions

In summary, we have investigated the water vapour uptake behaviour of a new generation of aqueous miscible organic layered double hydroxides. We found that the as prepared AMO-Zn_2MgAl–CO_3 and AMO-Mg_3Al–CO_3 exhibit high saturation water content of 21.6 and 11.7 wt% (on dry basis) respectively. The AMO-LDH with highest surface area and/or smallest particle size exhibits the greatest water vapour adsorption capacity. The majority of the adsorbed water was thought to reside in the interparticle region while some resides on the surface and in the interlayer galleries of LDH. The crystallite domain length in both *ab*-plane and *c*-axis increased with increasing water vapour exposure time. A simple surface modification method using stearic acid dramatically reduces the water vapour affinity an uptake rate, which should enable these highly dispersed materials to be used as additives in polymer composites and/or in pharmaceutical delivery systems.

Conflicts of interest

There are no conflicts to declare.

Acknowledgements

The authors would like to thank the surface analysis facility, University of Oxford, for use of the TGA and FTIR instruments. Dr Nicholas H. Rees (University of Oxford) is thanked for solid state NMR spectroscopy. C. Chen and J.-C. Buffet would like to thank SCG Chemicals Co., Ltd. (Thailand) for funding. K. Ruengkajorn would like to thank SCG Public Packaging Co., Ltd. (Thailand), for a graduate scholarship.

Notes and references

1 F. Cavani, F. Trifirò and A. Vaccari, *Catal. Today*, 1991, **11**, 173–301.
2 X. Duan and D. G. Evans, *Layered double hydroxides*, Springer Verlag, 2006.
3 V. Rives, *Layered double hydroxides: present and future*, Nova Publishers, 2001.
4 G. Fan, F. Li, D. G. Evans and X. Duan, *Chem. Soc. Rev.*, 2014, **43**, 7040–7066.
5 B. Sels, D. D. Vos, M. Buntinx, F. Pierard, A. Kirsch-De Mesmaeker and P. Jacobs, *Nature*, 1999, **400**, 855–857.
6 V. R. L. Constantino and T. J. Pinnavaia, *Catal. Lett.*, 1994, **23**, 361–367.
7 V. R. L. Constantino and T. J. Pinnavaia, *Inorg. Chem.*, 1995, **34**, 883–892.
8 A. Garcia-Gallastegui, D. Iruretagoyena, V. Gouvea, M. Mokhtar, A. M. Asiri, S. N. Basahel, S. A. Al-Thabaiti, A. O. Alyoubi, D. Chadwick and M. S. P. Shaffer, *Chem. Mater.*, 2012, **24**, 4531–4539.

9 M. Shao, F. Ning, J. Zhao, M. Wei, D. G. Evans and X. Duan, *J. Am. Chem. Soc.*, 2012, **134**, 1071–1077.
10 Y. Dou, S. Xu, X. Liu, J. Han, H. Yan, M. Wei, D. G. Evans and X. Duan, *Adv. Funct. Mater.*, 2014, **24**, 514–521.
11 F. Zhang, L. Zhao, H. Chen, S. Xu, D. G. Evans and X. Duan, *Angew. Chem., Int. Ed.*, 2008, **47**, 2466–2469.
12 Y. Dou, A. Zhou, T. Pan, J. Han, M. Wei, D. G. Evans and X. Duan, *Chem. Commun.*, 2014, **50**, 7136–7138.
13 Q. Wang and D. O'Hare, *Chem. Commun.*, 2013, **49**, 6301–6303.
14 C. Chen, A. Wangriya, J.-C. Buffet and D. O'Hare, *Dalton Trans.*, 2015, **44**, 16392–16398.
15 C. Chen, M. Yang, Q. Wang, J.-C. Buffet and D. O'Hare, *J. Mater. Chem. A*, 2014, **2**, 15102–15110.
16 V. Erastova, M. T. Degiacomi, D. O'Hare and H. C. Greenwell, *RSC Adv.*, 2017, **7**, 5076–5083.
17 M. Yang, O. McDermott, J.-C. Buffet and D. O'Hare, *RSC Adv.*, 2014, **4**, 51676–51682.
18 I. C. Smith, E. T. Hoke, D. Solis-Ibarra, M. D. McGehee and H. I. Karunadasa, *Angew. Chem., Int. Ed.*, 2014, **126**, 11414–11417.
19 Y. Yoo, V. Varela-Guerrero and H.-K. Jeong, *Langmuir*, 2011, **27**, 2652–2657.
20 Y. Uchida, S. Hishiya, N. Fujii, K. Kohmura, T. Nakayama, H. Tanaka and T. Kikkawa, *Microelectron. Eng.*, 2006, **83**, 2126–2129.
21 L. B. Rockland and G. F. Stewart, *Water activity: influences on food quality: a treatise on the influence of bound and free water on the quality and stability of foods and other natural products*, Academic Press, 2013.
22 A. Crouter and L. Briens, *AAPS PharmSciTech*, 2014, **15**, 65–74.
23 N. C. Burtch, H. Jasuja and K. S. Walton, *Chem. Rev.*, 2014, **114**, 10575–10612.
24 N. Iyi, K. Fujii, K. Okamoto and T. Sasaki, *Appl. Clay Sci.*, 2007, **35**, 218–227.
25 S. K. Yun and T. J. Pinnavaia, *Chem. Mater.*, 1995, **7**, 348–354.
26 X. Hou, D. L. Bish, S.-L. Wang, C. T. Johnston and R. J. Kirkpatrick, *Am. Mineral.*, 2003, **88**, 167–179.
27 J. C. Callahan, G. W. Cleary, M. Elefant, G. Kaplan, T. Kensler and R. A. Nash, *Drug Dev. Ind. Pharm.*, 1982, **8**, 355–369.
28 M. L. Occelli and H. Robson, *Expanded clays and other microporous solids*, Springer Science & Business Media, 2012.
29 J. T. Kloprogge, L. Hickey and R. L. Frost, *J. Raman Spectrosc.*, 2004, **35**, 967–974.
30 T. E. Johnson, W. Martens, R. L. Frost, Z. Ding and J. Theo Kloprogge, *J. Raman Spectrosc.*, 2002, **33**, 604–609.
31 Z. Cao, M. Daly, L. Clémence, L. M. Geever, I. Major, C. L. Higginbotham and D. M. Devine, *Appl. Clay Sci.*, 2016, **378**, 320–329.
32 H. Huang, M. Tian, J. Yang, H. Li, W. Liang, L. Zhang and X. Li, *J. Appl. Polym. Sci.*, 2008, **107**, 3325–3331.
33 L. Feng, H. Zhang, P. Mao, Y. Wang and Y. Ge, *Appl. Clay Sci.*, 2011, **257**, 3959–3963.
34 Q. Wang, B. Zhang, M. Qu, J. Zhang and D. He, *Appl. Clay Sci.*, 2008, **254**, 2009–2012.
35 P. D. Pudney, K. J. Mutch and S. Zhu, *Phys. Chem. Chem. Phys.*, 2009, **11**, 5010–5018.